**INFSO-ICT-216203 DAVINCI****D2.3.1 v1.0*****System level evaluation, Issue 1***

**Contractual Date of Delivery to the CEC:** 30 November 2008 (*as specified in the contract*)

**Actual Date of Delivery to the CEC:** 31 July 2009

**Author(s):** Alain Mourad, Ismael Gutierrez

**Participant(s):** SEUK

**Workpackage:** WP2

**Estimated person months:** 6

**Security:** PU

**Nature:** R

**Version:** 1.0

**Total number of pages:** 31

**Abstract:**

This deliverable presents the first results of system level evaluation using a WiMAX IEEE 802.16m-compliant system level simulator. The first results are obtained with IEEE 802.16m CTC codes only, since the available DAVINCI parity check matrices do not cover the configurations needed for system performance evaluation. Nevertheless, an analysis of DAVINCI codes versus CTC codes is conducted at the link to system interface level, where hints are given on their relative performance at the system level.

**Keyword list:** System Level Simulation, Link to System Interface, WiMAX IEEE 802.16m, Convolutional Turbo codes, DAVINCI codes

**Disclaimer:**

## Executive Summary

This report intends to quantify the performance of DAVINCI codes using system level performance metrics, which are essential to promote DAVINCI in the target IMT-Advanced standardization groups, namely, WiMAX IEEE 802.16m and 3GPP LTE-Advanced. For this purpose, according to Annex I of the Grant Agreement, a WiMAX IEEE 802.16m system level simulator has been developed. This simulator considers the release April 2009 of the WiMAX IEEE 802.16m system description document. An overview of this simulator is presented, highlighting its compliance with WiMAX IEEE 802.16m specification.

The Link to System Interface is particularly detailed by virtue of its major impact on the end system performance. This is also to enable identification of eventual adaptation of the Link to System Interface to the context of DAVINCI non-binary technology. A comparison between the DAVINCI codes and WiMAX IEEE 802.16m CTC codes is presented at the link to system interface, which gives insights on their relative performance at the system level.

The system level simulator is then used to evaluate the performance of reference WiMAX IEEE 802.16m CTC codes for the purpose of comparison and benchmarking. The DAVINCI codes could not be evaluated since the DAVINCI parity check matrices available do not cover the range of configurations (mainly in term of codeword size) needed for system performance evaluation. This is left for future evaluation in the forthcoming deliverable D2.3.2.

The main conclusions drawn out of this work show low expectation for a significant system improvement of DAVINCI codes relatively to WiMAX IEEE 802.16m CTC codes in the context linear receivers. This is due to the slight gain (up to 0.5 dB in the best case) observed for DAVINCI at the link to system interface. This gain might improve in the context of non-linear receivers. On another hand, we clearly show the need to implement CQI prediction mechanism in order to allow viable channel tracking by the scheduler for the scenarios with high CQI selectivity across the resource units.

## Authors

Partner	Name	Phone / Fax / e-mail
<b>Samsung Electronics UK (SEUK)</b>		
	Alain Mourad	Phone : +44 1784 600 Ext 756 Email : alain.mourad@samsung.com
	Ismael Gutierrez	Phone : +44 1784 600 Ext 780 Email : i.gutierrez@samsung.com

## Table of Contents

<b>1. INTRODUCTION .....</b>	<b>7</b>
<b>2. WIMAX IEEE 802.16M SYSTEM LEVEL SIMULATOR .....</b>	<b>8</b>
2.1 SLS CONFIGURATION.....	8
2.2 SLS INITIALIZATION .....	9
2.3 SLS SIMULATION .....	10
2.4 SLS EVALUATION .....	11
2.5 SLS COMPLIANCE WITH WIMAX IEEE802.16M.....	12
<b>3. LINK TO SYSTEM LEVEL INTERFACE.....</b>	<b>15</b>
3.1 QUALITY METRIC.....	15
3.2 COMPRESSION FUNCTION .....	16
3.3 MAPPING FUNCTION .....	17
3.4 DAVINCI vs. WIMAX CTC PERFORMANCE.....	19
<b>4. SYSTEM LEVEL RESULTS WITH WIMAX CTC SCHEME .....</b>	<b>21</b>
4.1 CONFIGURATION AND SCENARIOS .....	21
4.2 NUMERICAL RESULTS.....	22
4.2.1 CRU vs. DRU sub-channelization .....	22
4.2.2 SISO vs. SIMO reception.....	24
4.2.3 Low mobility vs. Medium mobility.....	27
<b>5. CONCLUSIONS AND PERSPECTIVES .....</b>	<b>30</b>

## List of Acronyms and Abbreviations

3GPP	3rd Generation Partnership Project
AMC	Adaptive Modulation and Coding
BS	Base Station
CDF	Cumulative Distribution Function
CP	Cyclic Prefix
CQI	Channel Quality Indicator
CTC	Convolutional Turbo Code
CRU	Contiguous Resource Unit
DAVINCI	Design And Versatile Implementation of Non-binary wireless Communications based on Innovative LDPC Codes
DC	Direct Current
DL	Downlink
DRU	Distributed Resource Unit
EMD	Evaluation Methodology Document
FDD	Frequency Division Duplex
FEC	Forward Error Correction
FFT	Fast Fourier Transform
FP7	Seventh Framework Programme
HARQ	Hybrid Automatic Repeat request
IEEE	Institute of Electrical and Electronics Engineers
IMT	International Mobile Telecommunications
LDPC	Low-Density Parity Check
LTE	Long Term Evolution
MCS	Modulation and Coding Scheme
MIMO	Multiple Input Multiple Output
MS	Mobile Station
OFDM	Orthogonal Frequency Division Multiplex
OFDMA	Orthogonal Frequency Division Multiple Access
RU	Resource Unit
QAM	Quadrature Amplitude Modulation
QPSK	Quadrature Phase Shift Keying
RRM	Radio Resource Management
RU	Resource Unit
SDD	System Description Document
SINR	Signal to Interference plus Noise Ratio
SISO	Single Input Single Output
SIMO	Single Input Multiple Output
SLS	System Level Simulator
SNR	Signal to Noise Ratio
TDD	Time Division Duplex
TGm	Task Group m, also called IEEE 802.16m
TTI	Transmission Time Interval
UL	Uplink
WiMAX	Worldwide Interoperability for Microwave Access
WP	Work Package

## Notations

$k$	index of the desired MS
$q$	index of BS ( $q = 0$ : Serving BS)
$a$	index of the BS transmit antenna $a$
$a_m$	$m$ -th constellation symbol
$b$	index of the MS receive antenna $b$
$M$	Constellation size
$N_{bs}$	Total number of BS in the system
$N_a$	Number of BS transmit antennas
$N_b$	Number of MS receive antennas
$N_s$	Number of data streams
$N_{di}^{(k)}$	Number of dominant BS interferers on desired MS index $k$
$I_{di}^{(k)}$	Set of indexes of the dominant BS interferers on desired MS index $k$
$I_{ndi}^{(k)}$	Set of indexes of the non - dominant BS interferers on desired MS index $k$
$A_q = \sqrt{2P_q \frac{N_{FFT}}{N_{USC}}}$	Amplitude of transmitted symbols by BS index $q$ , where $P_q$ is the power transmitted by BS index $q$ , and $N_{FFT}$ and $N_{USC}$ are respectively the FFT size and number of used sub-carriers carrying data and pilots
$\sigma^2 = 2N_0B$	Thermal noise power at MS receiver, where $2N_0$ is the two-sided noise spectral density, and $B$ is the system bandwidth
$G_{qk}$	Path gain for the link between BS index $q$ to MS index $k$
$h_{qk}^{(ab)}(n)$	Channel coefficient on sub-carrier $n$ for the link between transmit antenna index $a$ of BS index $q$ to receive antenna index $b$ of MS index $k$
$g_k(n)$	Equalizer coefficient on tone $n$ by MS index $k$
$r_k^{(b)}(n)$	Symbol received on tone $n$ on receive antenna index $b$ of MS index $k$
$s_q^{(a)}(n)$	Symbol carried on tone $n$ on transmit antenna index $a$ of BS index $q$
$w_k^{(b)}(n)$	Noise symbol received on tone $n$ at receive antenna index $b$ of MS index $k$
$Pu^{(k)}(n)$	Useful signal power on tone $n$ at MS index $k$
$Psi^{(k)}(n)$	Inter-symbol interference (in space-Time coding) power on tone $n$ at MS index $k$
$Pdi^{(k)}(n)$	Dominant inter-cell interference power on tone $n$ at MS index $k$
$Pndi^{(k)}(n)$	Non dominant inter-cell interference power on tone $n$ at MS index $k$
$Pn^{(k)}(n)$	Thermal noise power on tone $n$ at MS index $k$
$SINR^{(k)}(n)$	Instantaneous Signal to Interference plus Noise Ratio on tone $n$ at MS index $k$

## 1. Introduction

System level evaluation is essential to quantify the benefits of air interface technologies on the global system performance such as the system capacity, throughput, spectral efficiency, and coverage. At the system level, multiple links between multiple transmitters and receivers are considered in a multi-cellular environment, as opposed to the link level, where only the link between a transmitter and a receiver is considered.

The link level integrates the physical layer algorithms and evaluates their benefits on the link performance, primarily in terms of codeword error rate (CWER) vs. Signal to Noise Ratio (SNR). This is done in Task 2.2 of DAVINCI, where for instance, the DAVINCI encoder and decoder are integrated and compared to competing schemes from IMT-Advanced systems, namely, IEEE 802.16e/m, 3GPP LTE, and WINNER-II [DAV-D221].

On the other hand, the system level integrates upper layer mechanisms for resources allocation and management, whilst accounting for the specificity of the physical layer through so-called link to system interface. The benefits of physical layer and upper layer mechanisms are quantified on the system performance, primarily in terms throughput, delay, capacity, and coverage. The system level evaluation is essential to promote air interface technologies in standardization, as it quantifies their ultimate benefits on the overall system performance. This is the responsibility of task 2.3 in DAVINCI, which first outcome is planned in this first deliverable D2.3.1.

In order for the system level simulator (SLS) to quantify the benefits of DAVINCI technologies, it needs a full set of link performance for different codeword sizes, code rates, and modulation schemes. This is in order to properly account for the performance of different resource allocations and physical layer configurations decided by the scheduler, which is the heart of any SLS. Unfortunately this set is not yet available from DAVINCI. On another hand, in view of the ultimate goal of the system level evaluation to promote DAVINCI in IMT-Advanced standardization, particularly WiMAX IEEE 802.16m, it is quite important for the SLS development to comply with the specification of WiMAX IEEE 802.16m standard. This specification has been updated all along the past months.

In order not to delay further this deliverable, we decided to develop the SLS in compliance with the latest available release of April 2009 of WiMAX IEEE 802.16m system description document (SDD) [TGM-SDD]. Furthermore, since the available DAVINCI parity check matrices do not cover the needs of SLS for performance evaluation, we decided to provide in this deliverable the benchmark results with the competing coding scheme from WiMAX IEEE 802.16m, namely, the Convolutional Turbo Code (CTC). In order to give some insight onto the DAVINCI performance, we also give in this deliverable results available at the link level for comparing DAVINCI and CTC coding schemes.

This deliverable is structured as follows: **Section 2** provides an overview description of the WiMAX IEEE 802.16m system level simulator. **Section 3** presents the link to system interface with performance comparison between DAVINCI and CTC codes. This is to give an insight on their relative performance at the system level. **Section 4** gives the benchmark of system level results with CTC scheme for the specified simulation scenarios. Finally, **section 5** draws conclusions and provides directions for the way-forward for evaluating DAVINCI technologies at the system level.

## 2. WiMAX IEEE 802.16m System Level Simulator

The SLS developed by DAVINCI Partner SEUK follows the guidelines provided by WiMAX IEEE 802.16m evaluation methodology document [TGM-EMD] and system description document [TGM-SDD]. The main simulator components as specified in [TGM-EMD] are depicted in Figure 2-1. The SLS is developed for the downlink.

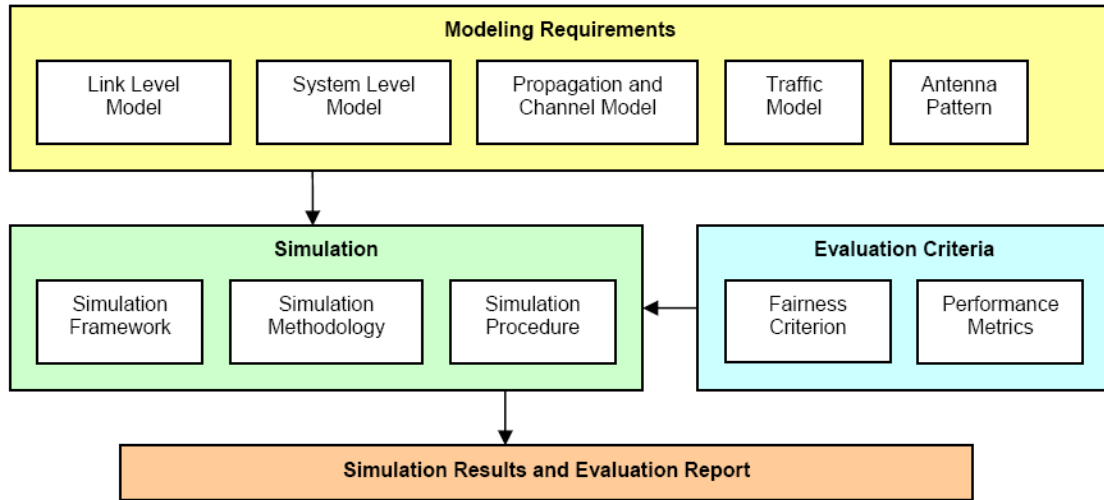


Figure 2-1: SLS architecture.

Figure 2-2 gives the flowchart at the functional level of the SLS. It consists of 4 main functions, namely, **configuration**, **initialization**, **simulation**, and **evaluation**. An overview of each of these functions is provided in the following subsections.

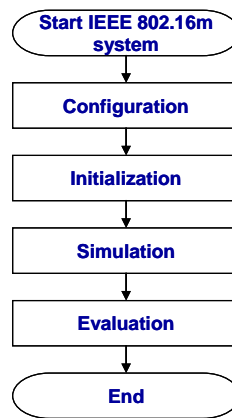


Figure 2-2: SLS functional flowchart.

### 2.1 SLS Configuration

Figure 2-3 depicts the functional flowchart of the SLS configuration. Four main categories of parameters are configured: **Simulation control**, **Cellular deployment**, **Propagation model**, and **Air interface**.

The **simulation control** sets the seeds for random generators and all the necessary parameters to control the Monte-Carlo simulation such as the number of snapshots and time interval for DL transmission per snapshot.

The **cellular deployment** covers the following:

- **Cellular topology** such as the numbers of cells and sectors per cell, the site to site distance, the number of mobile stations (MS) per sector.
- **BS and MS RF models** such as the transmit power per sector, height, antenna pattern, number of transmit and receive antennas, antenna spacing, noise figures, cable losses.

- **Traffic parameters** such as the traffic mix and QoS profiles per traffic (e.g. packet size, target FER, minimum data rate, priority, delay bound, etc.).

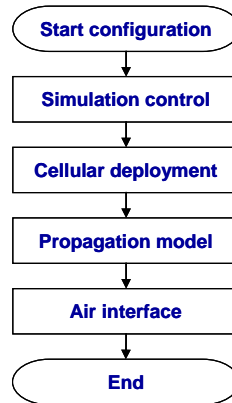


Figure 2-3: SLS configuration.

The **propagation model** specifies the following:

- **Large scale fading** such as the path loss model, shadowing model, penetration loss.
- **Small scale fading** such as the channel mix, channel profiles (e.g. ITU-Pedestrian B @3Kmh, ITU-Vehicular A@30Kmh, ITU-Vehicular A@120Kmh), spatial correlation.

The **air interface** defines the following:

- **OFDM modulator** such as the bandwidth, FFT size, guard interval size, sampling frequency, symbol duration, number of sub-carriers reserved for data and pilots.
- **MIMO scheme** such as the number of transmit and receive antennas, number of streams, space-time coding matrix, receiver type.
- **Frame structure** such as the number of frames per super-frame, number of sub-frame per frame, RTG and TTG durations, DL:UL ratio for TDD mode, types of sub-frames, number of OFDM symbols per type of sub-frame.
- **Sub-channelization** such as the number of resource units per sub-frame, number of sub-carriers per resource unit, pilot patterns per resource unit, permutation tables.
- **Scheduling** such as the type of scheduler algorithm, latency time scale, latency factor, fairness factor, FER threshold, type of CQI, CQI feedback.
- **Modulation and coding** such as the constellations, coding schemes, coding rates, codeword sizes, available for adaptive coding and modulation.
- **H-ARQ** such as the type, maximum number of retransmissions, retransmission delay.

## 2.2 SLS Initialization

Figure 2-4 depicts the functional diagram of SLS initialization. It calls functions to initialize the following:

- **Cellular deployment** which creates the cellular infrastructure with wrap-around (e.g. BS locations and service area) and assigns antenna patterns to the sectors.
- **Time-variant fast fading** which for each channel model normalized the power delay profile and sets corresponding parameters (Jakes Doppler spectrum, frequency ranges, etc.) for the time-variant channel according to the channel Doppler frequency.
- **Sub-channelization** which generates the outer-permutation of the resource units per sector, distributes the contiguous (CRU) and distributed (DRU) resource units across the sectors according to an outer-loop static scheduler, generates the inner permutations per for the block of DRU per OFDM symbol (according to standard specification), and pre-computes data and pilots indexes per symbol per sector.

- **Link to system interface** which loads the Look-Up Tables (LUT) mapping the symbol level mutual information to the post-processing SINR per constellation, and LUT mapping on AWGN channel the CWER to SNR per modulation and coding scheme and codeword size. This corresponds to the RBIR mandatory link to system mapping adopted in WiMAX 16m.

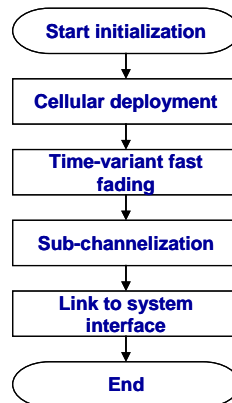


Figure 2-4: SLS initialization.

Figure 2-5 illustrates the cellular layout with 19 3-sectored cells and wrap-around technique. A wrap-around enables to create symmetrical conditions as in a system with infinite number of cells. Six copies of the main cluster are created for this purpose as shown below. This allows for data collection from all the cells in the central cluster since all these cells are central cells and experience equivalent interference conditions. This implementation guarantees high accuracy for the output statistics at reduced overall computational complexity. The service area is defined with the rhombus shown in Figure 2-5. The MS are dropped in this service area randomly with a uniform distribution and their positions are then recalculated with respect to the central cluster using the wrap-around model.

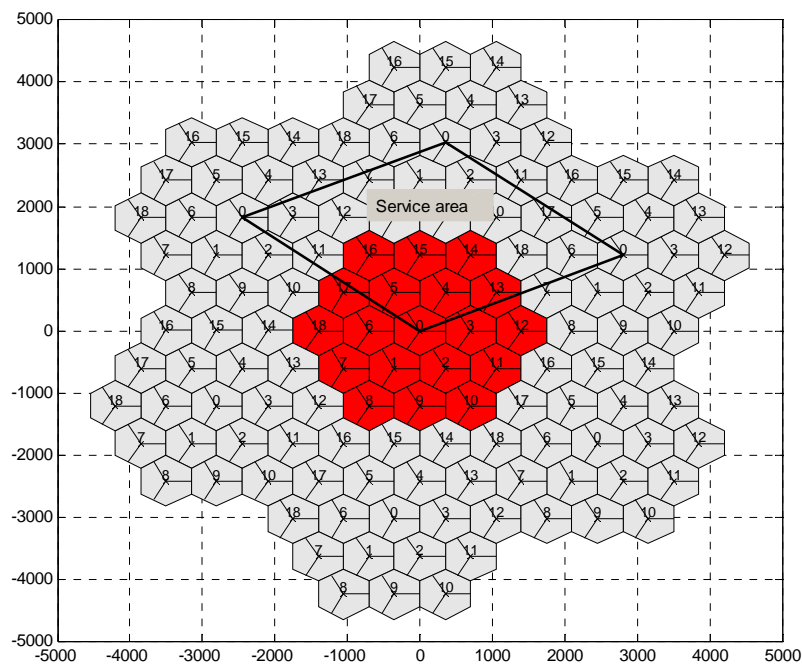


Figure 2-5: Cellular layout with 19 3-sectored cells and wrap-around.

### 2.3 SLS Simulation

Figure 2-6 depicts the functional flowchart of the SLS simulation. It consists in a first loop on the number of snapshots where a given realization of MS dropping in the service area is generated, and a second loop where the DL transmission for the different active links is simulated.

The **MS dropping** function drops the MS uniformly in the service area and then computes their relative locations to the main cluster. It ensures each sector has the fixed number of MS set in the configuration, where each MS respects the minimum distance constraint from the BS. The assignment of MS to the serving sector is done according to the maximum path gain criterion. No macro-diversity is assumed, i.e. a MS is connected to only one sector. Moreover, this function assigns to each dropped MS a traffic and channel model according to the traffic and channel mixes respectively. It also determines a set of dominant interfering sectors for which the path gains to the given MS exceed a given threshold relatively to the path gain of the MS to its serving sector.

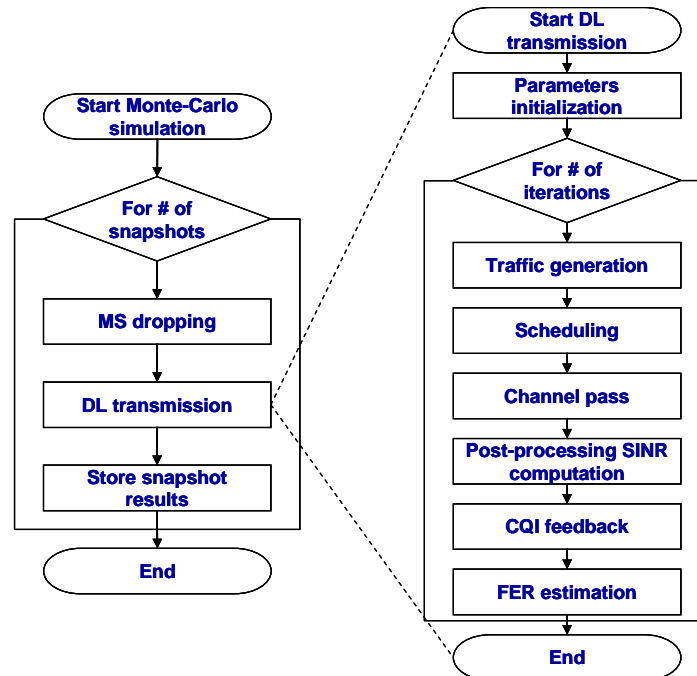


Figure 2-6: SLS simulation.

The **DL transmission** first initializes parameters evolving along the transmission period (e.g. initial CQI values, initial average throughput, frequency noise generators, etc.). It then starts transmission frame per frame following the frame structure defined in the configuration and TDD duplex parameters. The traffic generation is first updated. Then the scheduler of each sector takes decision as regarding which resource units to be assigned to which active MS at which modulation and coding schemes.

The transmission is then modeled by the channel pass, which first generates the fast fading physical channels for the links between the MS and its serving sector and dominant interfering sectors. The physical channels are then transformed into equivalent channels according to the sub-channelization configuration (thus performing the physical to logical sub-channels mapping).

The MS then computes the per data symbol post-processing SINR for the specified MIMO mode and all resource units over the whole bandwidth. It then determines the CQI per logical resource unit for feedback to the scheduler. The MS finally uses the link to system interface tables to estimate the FER associated with the current transmission.

H-ARQ is not implemented in the current version. It will follow in the next version of the SLS.

All performance metrics are stored on per iteration and per snapshot basis into output files for offline processing later by the performance evaluation function.

## 2.4 SLS Evaluation

Figure 2-7 depicts the functional diagram of SLS evaluation. It does the following:

- **Load the performance files** obtained per snapshot and iteration from the SLS simulation.
- **Compute scheduler metrics** such as the average number of MS scheduled per sector, the average number of resource units scheduled per MS, percentage of scheduled Contiguous and Distributed resource units, percentage of scheduled modulation and coding schemes, average scheduled throughput per MS and per sector.

- **Compute receiver metrics** such as the average received SINR, the average measured throughput per MS and per BS, the average measured CWER and FER, the average CQI per resource unit per iteration and per MS, distances of MS to serving BS, etc.
- **Output statistical results** which outputs the cumulative distribution functions (CDF) of the scheduler and receiver metrics, outage values at given percentile of the CDF, percentages of use per distance, etc.

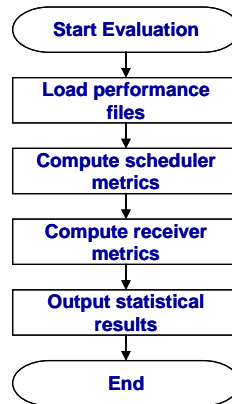


Figure 2-7: SLS evaluation.

## 2.5 SLS compliance with WiMAX IEEE802.16m

Table 2-1 and Table 2-2 describe the SLS features and its compliance with WiMAX IEEE802.16m baseline specification.

Table 2-1: SLS deployment features and compliance with WiMAX 16m.

Feature	Description	16m - EMD (Baseline)	P01 SEUK - SLS
Topology	Network topology for cellular deployment	Network of 7 clusters with wraparound, each cluster 19 cells, each cell of three sectors	16m compliant
MS dropping	Dropping MSs in the service area	Following a uniform distribution throughout the service area Users dropped within 35 m of a sector antenna shall be redropped	16m compliant
Sector load	Number of users per sector	Continuous drop until the desired fixed number of users per sector is achieved. Each user is assigned to only one sector for counting purposes	16m compliant
Channel mix	MSs channel models assignment	Fixed for all MS or Mixed scenario Random channel models according to channel model mix or Random channel realizations of a single type of channel model	16m compliant
Shadowing correlation	Inter-site correlation and shadowing correlation distance	Inter-site correlation equal to 0.5 and shadowing correlation distance equal to 50 m	Inter-site correlation equal to 0.5 but no shadowing correlation distance
Traffic mix	MSs traffic profiles assignment	Following specified traffic mix	16m compliant
Simulation time	Necessary time to end simulation and output overall performance results	Simulation time for each drop should ensure convergence in the user performance metrics. A sufficient number of drops are simulated to ensure convergence in the system performance metrics	16m compliant
Statistics collection	Collection of statistics from simulated MSs and sectors	Collection from all MSs in all 57 sectors (wraparound)	16m compliant
Channel model	Ray-based (summing over multiple rays: 3GPP, SCM, SCME, WINNER) or Correlation-based (analytical PAP modeling of statistical behaviour of the channel)	Correlation-based with spatial correlation specific to each user but same for all taps	16m compliant (case 1: spatially uncorrelated channels)
Interference model	Co-channel interference model, fading model for interferers, number of major interferers, threshold receiver, interference awareness	From each MS into each sector and from each sector to each MS for each simulation interval - Same fast fading channel model but different realizations to each link between an MS and all BSs in the network - Generate fast fading channel realizations for strong interferers	16m compliant
Channel estimation model	Model to account for the impact of channel estimation errors on the performance	Effective noise variance equal to noise variance plus MSE of channel estimation errors	None
PHY model	PHY abstraction method: EESM, MMB, RBIR, etc.	RBIR	16m compliant
Traffic model	MS traffic arrival processes and service profiles	Full queue	16m compliant
Mobility model	Single or multiple moving MS models for MS trajectories and velocities	Location of each MS remains unchanged during a drop. The speed of an MS is only used to determine the Doppler effect of fast fading	16m compliant
Error Vector Magnitude	Models impact of PAPR reduction methods on transmitted waveform quality	Post-processing SINR is modified for accounting of EVM	None

Table 2-2: SLS air interface features and compliance with WiMAX IEEE 802.16m.

Feature	Description	16m - EMD (Baseline)	P01 SEUK - SLS
Link direction	DL, UL	DL	16m compliant
Duplexing scheme	TDD, FDD	TDD	16m compliant
Multiple access	Multiple access scheme	OFDMA	16m compliant
Subchannelization	Sub-carrier permutation	Contiguous and Distributed resource units (CRU and DRU)	16m compliant
Resource allocation granularity	Smallest unit of resource allocation	18 sub-carriers x 5 OFDM symbols (sub-frame of type 3)	16m compliant
Basic modulation	Modulation schemes for data and control	QPSK, 16QAM, 64QAM	16m compliant
Data channel coding	Channel coding schemes	Convolutional Turbo Coding (CTC)	16m compliant
Multi-antenna Transmission Format	Multi-antenna configuration and transmission scheme	MIMO (2x2) (Adaptive MIMO switching matrix A & matrix B) Beamforming (2x2)	16m compliant except no adaptive MIMO nor beamforming
Pilot structure	Pilot structure, density etc.	Specific to the subchannelization scheme and MIMO mode	16m compliant
Receiver structure	MMSE/ML/MRC/Interference cancellation	MMSE (Matrix B data zone), MRC (Matrix A data zone)	16m compliant
AMC	Adaptive Modulation and Coding	QPSK (1/2) with repetition 1/2/4/6, QPSK (3/4) 16QAM (1/2, 3/4) 64QAM (1/2, 2/3, 3/4, 5/6)	QPSK (1/2, 2/3, 3/4, 5/6) 16QAM (1/2, 2/3, 3/4, 5/6) 64QAM (1/2, 2/3, 3/4, 5/6)
H-ARQ	Chase combining, incremental redundancy, synchronous/asynchronous, adaptive/non-adaptive, ACK/NACK delay, Maximum number of retransmissions, retransmission delay	Chase combining asynchronous, non-adaptive, 1 frame ACK/NACK delay, ACK/NACK error, maximum 4 HARQ retransmissions, minimum retransmission delay 2 frames	None
Channel Quality Feedback	Channel quality indicators, feedback delay, feedback rate, feedback error	CQI = Effective SINR per resource unit, no feedback delay, no prediction errors	16m compliant
Spatial adaptation	Antenna selection, switching MIMO schemes, etc.	Adaptive MIMO switching matrix A & matrix B	None
Power loading	Sub-carrier power allocation	Equal power	16m compliant
Scheduling	The scheduler allocates system resources for different packet transmissions according to a set of scheduling metrics. The scheduling metric is traffic specific and accounts for the reported metrics (CQI and other metrics)	Proportional fairness for full buffer data only 10 active users per sector	16m compliant
Cell selection	Cell selection via scanning and network entry including synchronization and ranging with a target BS	Serving sector has the best path to MS in term of long-term slow fading received power	16m compliant
Handover	Cell reselection via scanning, handover decision and initiation, and synchronization and ranging with a target BS	Intra-radio access technology HO is considered but not inter-radio access technology HO	None
Power control	Open loop / Closed loop	Maximum power	16m compliant
Interference management	Interference power control, coordination, randomization, suppression	None	None
Frequency reuse	Frequency reuse pattern	Frequency reuse of 1	16m compliant
Multi-band management	Multi-band selection and scheduling procedures	None	None

### 3. Link to System Level Interface

The role of the **Link to System level Interface** (L2S) is to predict the link performance based on metrics accessible at the system level. It represents the alternative to the prohibitive complexity solution of overall link level processing for all the different links considered at the system level. It also defines metrics for use by channel-aware scheduling and adaptation mechanisms in real systems.

Two classes of L2S have been considered in the literature: **Average-value interface** and **Actual-value interface**. The resolution of the **average-value interface** is low so that the effects of small-scale channel conditions are modeled in average values over a large observation time interval compared to the channel coherence time (e.g. hundreds of Transmission Time Interval (TTI)). On the opposite, the **actual-value interface** considers a high resolution such that the effects of small-scale channel conditions are modelled in actual or instantaneous values, i.e. an observation of one or few TTIs. This latter interface is more suitable for mechanisms exploiting short term or instantaneous channel knowledge such as fast channel-aware scheduling and link adaptation. In this work, we only consider the actual-value interface since our objective is to evaluate the DAVINCI technologies into WiMAX IEEE 802.16m SLS with channel-aware scheduling and adaptation capability.

A three-step approach is commonly used to define the actual-value L2S interface:

1. Define **quality metrics** according to the SLS resolution. These metrics should capture the transceiver features and preserve the relative merits of transceiver algorithms. Examples of quality measures are **post-processing SINR** and instantaneous channel capacity.
2. Define a **compression function** in order to easily map the large number of quality metrics corresponding to the several multi-dimensional (i.e. space, time, frequency, etc.) resource elements used to carry the codeword. After compression, the number of metrics reduces to one or two, e.g. average and variance SINR over the codeword.
3. Define a **mapping function** between the metrics after compression and the codeword error rate (CWER). This mapping is generally taken on AWGN channel and hence only dependent on the modulation and coding scheme (MCS) and codeword length.

Several models have been proposed in the literature. In WiMAX IEEE 802.16m, the three most common ones are considered, namely, the Exponential Effective SINR (EES), Received Bit Information Rate (RBIR), and Mean Mutual Information per coded Bit (MMIB). The **RBIR** is selected as **mandatory**, whereas the others are left as optional. In our SLS, we implement the RBIR model for the sake of compliancy with WiMAX IEEE 802.16m, and thus we give it special attention in the sequel.

#### 3.1 Quality Metric

In the context of **linear receivers**, all models assume the per-data symbol **post-processing SINR** (e.g. after space-time-frequency decoding) across the codeword to capture the link performance and thus enable to predict the CWER. Things become more complicated in the context of **non-linear receivers** (e.g. Maximum Likelihood), where the post-processing SINR per data symbol is not accessible. In this latter context, some models (e.g. EES) fail to extend, while others (e.g. RBIR and MMIB) based on the **Mutual Information** succeeds to provide a tentative solution. Here, we only consider linear receivers, and hence the metric of post-processing SINR per data symbol. Figure 3-1 depicts the post-processing SINR-based L2S model.

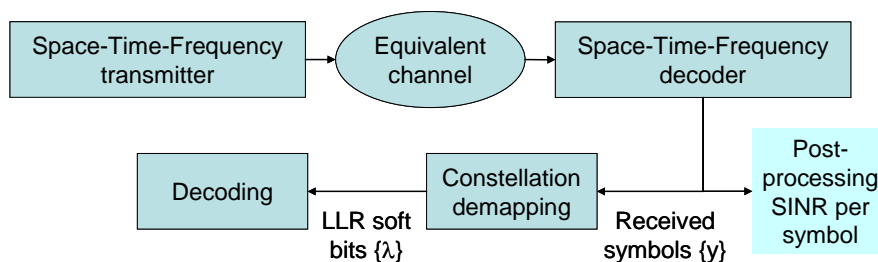


Figure 3-1: Post-processing SINR-based model.

At the system level, the received symbol on  $n$ -th tone and  $b$ -th receive antenna at  $k$ -th MS is obtained as (see notations defined on page 7):

$$\begin{aligned}
r_k^{(b)}(n) = & \sqrt{G_{0k}} \sum_{a=0}^{N_a-1} h_{0k}^{(ab)}(n) s_0^{(a)}(n) + \sum_{q \in I_{di}^{(k)}} \sqrt{G_{qk}} \sum_{a=0}^{N_a-1} h_{qk}^{(ab)}(n) s_q^{(a)}(n) \\
& + \sum_{q \in I_{ndi}^{(k)}} \sqrt{G_{qk}} \sum_{a=0}^{N_a-1} s_q^{(a)}(n) + w_k^{(b)}(n)
\end{aligned} \tag{1}$$

The post-processing SINR for the  $n$ -th tone at  $k$ -th MS receiver is generally expressed as:

$$SINR_k(n) = \frac{Pu_k(n)}{Psi_k(n) + Pdi_k(n) + Pndi_k(n) + Pn_k(n)} \quad ; \quad \forall n = 1 \dots N \tag{2}$$

Obviously, different expressions exist for different transmitter and receiver models. Here, we just give the expressions of the post-processing SINR for the two modes considered in the performance evaluation conducted in next section 4

In the SISO (1 x 1 antenna configuration) with MRC receiver, the post-processing SINR is obtained as:

$$SINR_k(n) = \frac{G_{0k} |h_{0k}(n)|^2 A_0^2}{\sum_{q \in I_{di}^{(k)}} G_{qk} |h_{qk}(n)|^2 A_q^2 + \sum_{q \in I_{ndi}^{(k)}} G_{qk} A_q^2 + \sigma^2} \tag{3}$$

In the SIMO (1 x  $N_b$  antenna configuration) with MRC receiver, it becomes:

$$SINR_k(n) = \frac{A_0^2 G_{0k} \left( \sum_{b=0}^{N_b-1} |h_{0k}^{(b)}(n)|^2 \right)^2}{\sum_{q \in I_{di}^{(k)}} A_q^2 G_{qk} \left| \sum_{b=0}^{N_b-1} h_{0k}^{(b)*}(n) h_{qk}^{(b)}(n) \right|^2 + \sum_{q \in I_{ndi}^{(k)}} A_q^2 G_{qk} \left| \sum_{b=0}^{N_b-1} h_{0k}^{(b)*}(n) \right|^2 + \sigma^2 \sum_{b=0}^{N_b-1} |h_{0k}^{(b)}(n)|^2} \tag{4}$$

Other expressions have been implemented in the SLS covering most relevant MIMO modes in WiMAX IEEE 802.16m with the matrix A (Space-Time Coding) and matrix B (Spatial multiplexing), MRC and MMSE receivers, {2 x 1, 2 x 2, 4 x 2} MIMO configurations. Details will be provided in next deliverable D2.3.2 when system performance evaluation will be conducted with these modes.

In the sequel, we remove the MS index  $k$  for the sake of clarity.

### 3.2 Compression function

The  $N$  multi-state SINR values across the codeword are compressed into an effective SINR, which is mapped to the CWER through the mapping function. Obviously, the CWER not only depends on the average value but on the entire statistics of the SINR and correlation in case of non-ideal interleaving. A generalized formulation of the effective SINR is given hereafter:

$$CWSINR = I^{-1} \left( \frac{1}{N} \sum_{n=0}^{N-1} I(SINR(n)) \right) \xleftarrow{\text{one-to-one-mapping}} CWER \tag{5}$$

Where the function  $I(x)$  is referred to as information measure and  $I^{-1}(x)$  is its inverse. It is worth pointing out that the inverse  $I^{-1}$  mainly influences the shape of the mapping function and not (or only to a small extent) the accuracy of CWER prediction.

In the following, we only present the information measure corresponding to the RBIR model. The RBIR model assumes one-to-one mapping between the average mutual information across the codeword and CWER. This is shown hereafter:

$$CWMI = \frac{1}{N} \sum_{n=0}^{N-1} I(d(n); \tilde{d}(n)) \xleftarrow{\text{one-to-one-mapping}} CWER \tag{6}$$

Where the data symbol received on  $n$ -th tone is modelled as:

$$\tilde{d}(n) = d(n) + \tilde{w}(n) \quad (7)$$

In the following, we remove the tone index  $n$  for the sake of clarity. Assuming the interference plus noise term to follow a Gaussian distribution, and defining the variable  $\theta$  as:

$$\theta = \tilde{d} - a_m = (d - a_m) + \tilde{w} \propto N\left(0, \frac{1}{\text{SINR}}\right) \quad (8)$$

The symbol level mutual information can then be derived as:

$$I(d; \tilde{d}) = \log_2(M) - \frac{1}{M} \sum_{m=0}^{M-1} E \left( \log_2 \left( \sum_{\ell=0}^{M-1} \exp \left( -\frac{|\theta + a_\ell - a_m|^2 - |\theta|^2}{(1/\text{SINR})} \right) \right) \right) \quad (9)$$

Where  $M$  and  $\{a_m\}$  are respectively the size and symbols of the constellation used for data transmission on the  $n$ -th tone.

The RBIR is then obtained as:

$$\text{RBIR} = \frac{\sum_{n=0}^{N-1} I(\text{SINR}(n))}{\sum_{n=0}^{N-1} M(n)} \quad (10)$$

The RBIR value encompasses all the variation of the quality of the bits within the codeword. It is the value reflecting the quality of the codeword. It is invariant with the MCS needed to predict the CWER. Thus, it can be fed back to the scheduler for MCS selection.

Thus, in order to determine the information measure per tone, we need to input its corresponding post-processing SINR to the LUT mapping in (9), which is modulation-specific. Figure 3-2 illustrates the LUT in (9) mapping the symbol level mutual information to the post-processing SINR for QPSK, 16QAM, and 64QAM modulations.

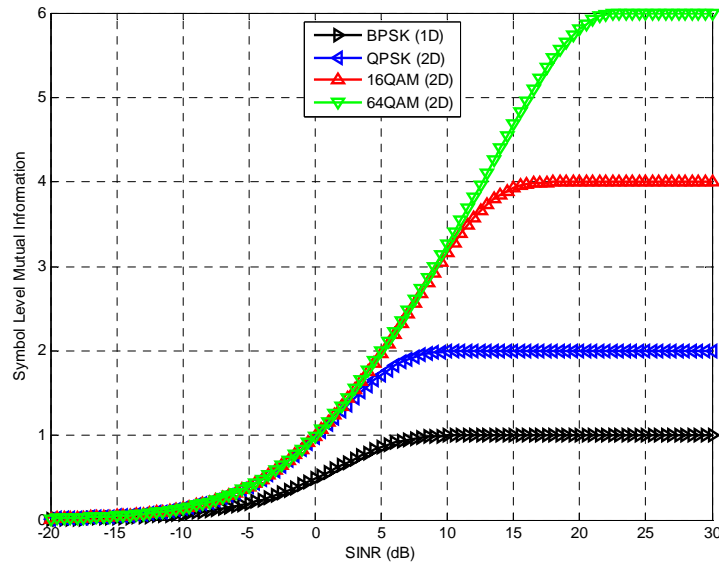


Figure 3-2: Symbol Level Mutual Information vs. SINR for different constellations.

### 3.3 Mapping function

The mapping between effective SINR and CWER is obtained on AWGN channel for given modulation and coding scheme and codeword length. It is derived with AWGN link level simulation or associated

polynomial approximation. Knowing the effective SINR representative of the quality of the codeword, the CWER is then predicted simply from the LUT mapping the SNR to CWER on AWGN channel with the effective SINR as input.

For WiMAX IEEE 802.16m CTC, we choose the following MCS schemes:

Table 3-1: Modulation and coding schemes.

MCS	Modulation	Coding Rate
{1,2,3,4}	QPSK	{1/2,2/3,3/4,5/6}
{5,6,7,8}	16QAM	{1/2,2/3,3/4,5/6}
{9,10,11,12}	64QAM	{1/2,2/3,3/4,5/6}

For the codeword lengths, in order to limit the number of SNR-to-CWER mappings to be generated and stored, we consider codeword lengths up to 4 resource units (i.e. 408 QAM symbols). For resource allocation of more than 4 resource units, we assume the same LUT as for 4 resource units. This assumption is motivated by the small difference in SNR to CWER mappings for high codeword lengths. But this is yet to be confirmed.

The following configurations are considered for SNR-to-CWER mappings.

1 RU	Code Word length Nq (QAM symbols)	102			
	Constellation type	QPSK			
	Constellation size	4			
	Code Rate	1/2	2/3	3/4	5/6
	Word length Kb (information bits)	102	136	153	170
	Closest Kb available	102	136	144	160
	Constellation type	16QAM			
	Constellation size	16			
	Code Rate	1/2	2/3	3/4	5/6
	Word length Kb (information bits)	204	272	306	340
	Closest Kb available	208	272	312	320
	Constellation type	64QAM			
	Constellation size	64			
	Code Rate	1/2	2/3	3/4	5/6
Word length Kb (information bits)	306	408	459	510	
Closest Kb available	304	408	456	480	

2 RU	Code Word length Nq (QAM symbols)	204			
	Constellation type	QPSK			
	Constellation size	4			
	Code Rate	1/2	2/3	3/4	5/6
	Word length Kb (information bits)	204	272	306	340
	Closest Kb available	208	272	312	360
	Constellation type	16QAM			
	Constellation size	16			
	Code Rate	1/2	2/3	3/4	5/6
	Word length Kb (information bits)	408	544	612	680
	Closest Kb available	408	544	624	640
	Constellation type	64QAM			
	Constellation size	64			
	Code Rate	1/2	2/3	3/4	5/6
Word length Kb (information bits)	612	816	918	1020	
Closest Kb available	608	816	912	960	

3 RU	Code Word length Nq (QAM symbols)	306			
	Constellation type	QPSK			
	Constellation size	4			
	Code Rate	1/2	2/3	3/4	5/6
	Word length Kb (information bits)	306	408	459	510
	Closest Kb available	304	408	456	480
	Constellation type	16QAM			
	Constellation size	16			
	Code Rate	1/2	2/3	3/4	5/6
	Word length Kb (information bits)	612	816	918	1020
	Closest Kb available	608	816	912	960
	Constellation type	64QAM			
	Constellation size	64			
	Code Rate	1/2	2/3	3/4	5/6
Word length Kb (information bits)	918	1224	1377	1530	
Closest Kb available	912	1216	1440	1600	

4 RU	Code Word length Nq (QAM symbols)	408			
	Constellation type	QPSK			
	Constellation size	4			
	Code Rate	1/2	2/3	3/4	5/6
	Word length Kb (information bits)	408	544	612	680
	Closest Kb available	408	544	624	640
	Constellation type	16QAM			
	Constellation size	16			
	Code Rate	1/2	2/3	3/4	5/6
	Word length Kb (information bits)	816	1088	1224	1360
	Closest Kb available	816	1088	1248	1280
	Constellation type	64QAM			
	Constellation size	64			
	Code Rate	1/2	2/3	3/4	5/6
Word length Kb (information bits)	1224	1632	1836	2040	
Closest Kb available	1216	1632	1824	1920	

The resulting SNR-to-CWER mappings are illustrated in Figure 3-3 below.

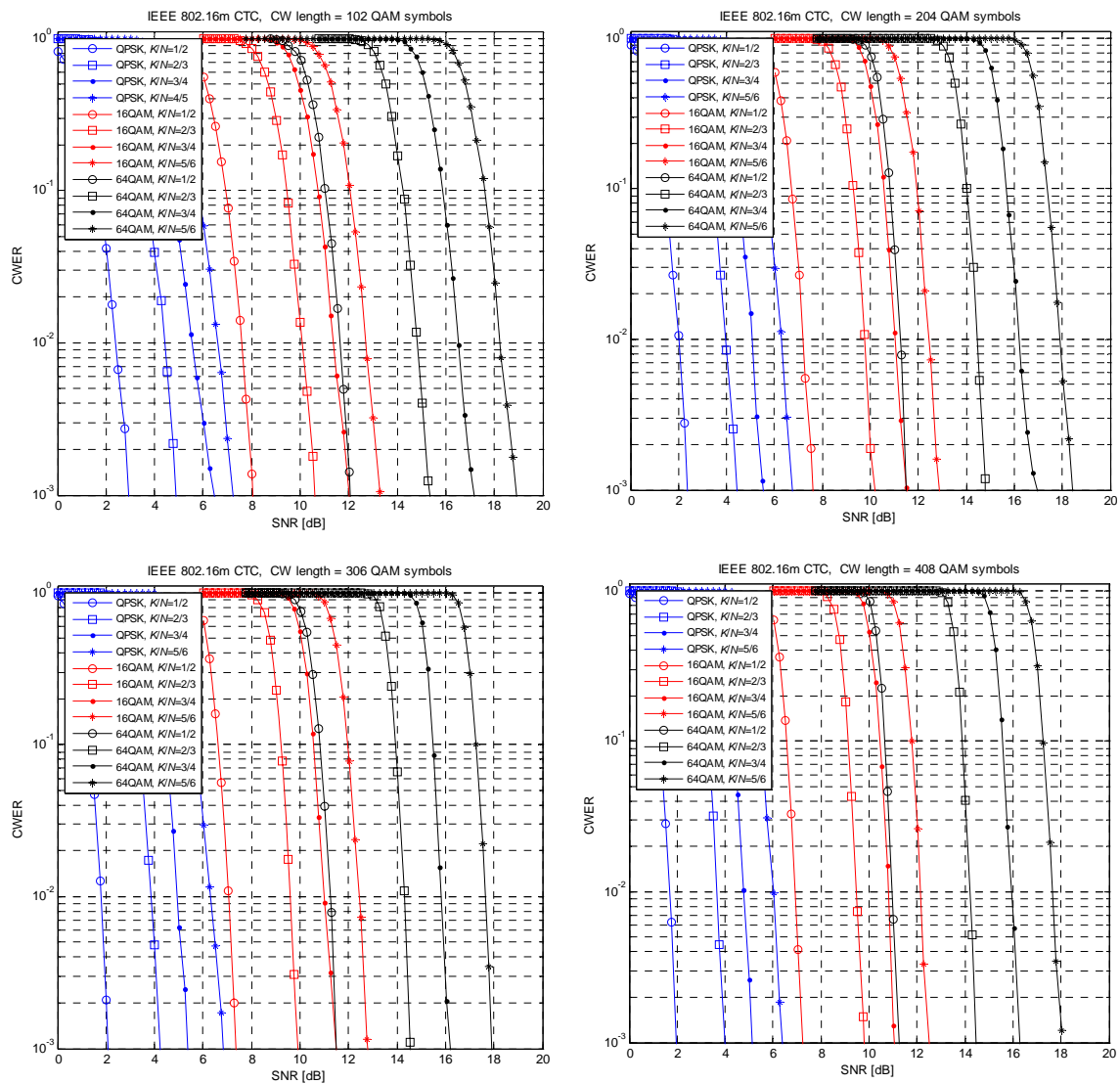


Figure 3-3: SNR-CWER LUTs for WiMAX IEEE 802.16m CTC scheme.

### 3.4 DAVINCI vs. WiMAX CTC performance

Figure 3-4 shows the CWER-to-SNR mappings for DAVINCI and WiMAX CTC codes for closest available codeword sizes in terms of number of QAM symbols, specifically 288 QAM for DAVINCI and 306 for CTC. All MCS schemes in Table 3-1 are considered.

From Figure 3-4, we can see DAVINCI codes are slightly better for all configurations. The gain achieved by DAVINCI codes is nearly 0.5 dB at the best case. This small gain will convert into an even smaller

gain in terms of system level performance. The performance of DAVINCI codes at the system level is therefore very likely to be similar than WiMAX CTC codes.

As DAVINCI codes are expected to provide better performance for higher codeword sizes, the performance gain at the system level might improve a little in favour of DAVINCI. But this is yet to be evaluated and confirmed.

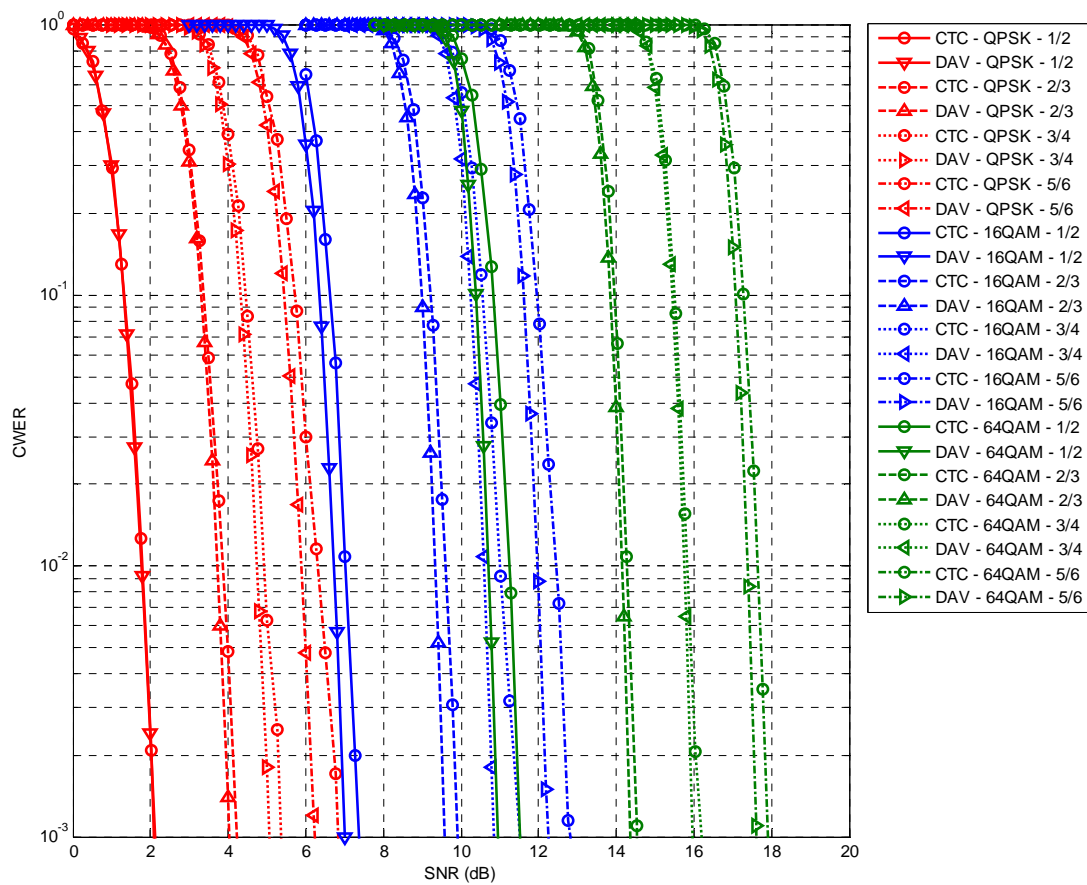


Figure 3-4: SNR-CWER LUTs for DAVINCI (288 QAM symbols) and WiMAX IEEE 802.16m CTC scheme (306 QAM symbols).

Since we only consider here the context of linear receivers, DAVINCI non-binary codes might be more suitable to non-linear receivers. It is therefore possible that DAVINCI achieves higher gain than WiMAX CTC codes with non-linear receivers. This has to be yet confirmed first at the link level, and then an adequate design of the L2S interface can take place in order to convert this gain properly at the system level. This is left for further investigation.

## 4. System level results with WiMAX CTC scheme

The system level results presented in this Chapter are obtained with the L2S LUT presented in section 3 for WiMAX CTC scheme.

### 4.1 Configuration and scenarios

Table 4-1 gives the most relevant configuration parameters used for system level simulations.

Table 4-1: Main SLS configuration parameters.

Parameter	Value	Parameter	Value
<b>Deployment</b>		<b>Air Interface</b>	
Site-to-Site distance	1.5 Km	Carrier frequency	2.5 GHz
Number of cells	19	Nominal channel bandwidth	10 MHz
Wrap-around	Yes	Number of used sub-carriers including DC	721
Number of sectors per cell	3	Cyclic prefix ratio	1/8
Minimum distance to base station	35 m	Frame duration	5 ms
BS maximum transmit power	46 dBm	Number of sub-frames per frame	8
BS antenna maximum gain	17 dBi	DL:UL ratio	5:3
BS antenna beamwidth @3dB	70 deg.	TTG time	102.857 $\mu$ s
BS antenna front-to-back ratio	20 dB	RTG time	62.857 $\mu$ s
MS antenna maximum gain	0 dBi	Number of sub-carriers per RU	18
MS receiver noise figure	7 dB	Number of RU	40
MS receiver cable loss	0 dB	PF scheduler latency time scale	5 ms
MS Thermal noise density	-174 dBm/Hz	PF scheduler latency scale in RU	10 RU
Path loss model	Loss (dB) = 130.19 + 37.6log10(R) (R in Km)	PF scheduler fairness exponent factor	1
Building Penetration loss	10 dB	AMC FER threshold	1E-02
Shadowing standard deviation	8 dB	AMC modulations	QPSK, 16QAM, 64QAM
Shadowing site-to-site correlation	0.5	AMC coding rates	1/2, 2/3, 3/4, 5/6
Dominant interferer threshold	10 dB	AMC codeword sizes (QAM symbols)	102, 204, 306, 408
Channel mix	M-Ped B@3Kmh M-VehA@30Kmh M-VehA@120Kmh	CQI metric	Effective Mutual Information (EMI)

We consider the following main simulation parameters: 10 users per sector, 3 snapshots, and transmission of 50 frames per snapshot (i.e. transmission time of 0.25 sec). Although short, the transmission time enables almost stable results with the PF scheduler latency of 10 (thus average ratio of 1/10).

Table 4-2 gives the scenarios considered for SLS baseline results. We mainly consider the effect of contiguous and distributed sub-channelization, SISO and SIMO schemes, low and medium mobility (Pedestrian B@3Kmh and Vehicular A@30Kmh). The SLS allows very wide range of scenarios covering

the channel mix, traffic mix, sophisticated MIMO modes, CRU/DRU mix, etc. We decided to restrict the SLS results presented in this report to the simple ones to ease the understanding of the results and allows for ease benchmarking later on with DAVINCI schemes.

Table 4-2: SLS baseline scenarios.

Scenario no.	MIMO mode	Channel mix	Subchannelization
A1	SISO - MRC	M-PedB3	CRU
A2	SISO - MRC	M-PedB3	DRU
B1	SIMO - MRC	M-PedB3	CRU
B2	SIMO - MRC	M-PedB3	DRU
C1	SISO - MRC	M-VehA30	CRU
C2	SISO - MRC	M-VehA30	DRU

## 4.2 Numerical results

### 4.2.1 CRU vs. DRU sub-channelization

Figure 4-1 to Figure 4-5 show statistics for different performance metrics comparing the scenario A1 with contiguous RU (CRU) to scenario A2 with distributed RU (DRU).

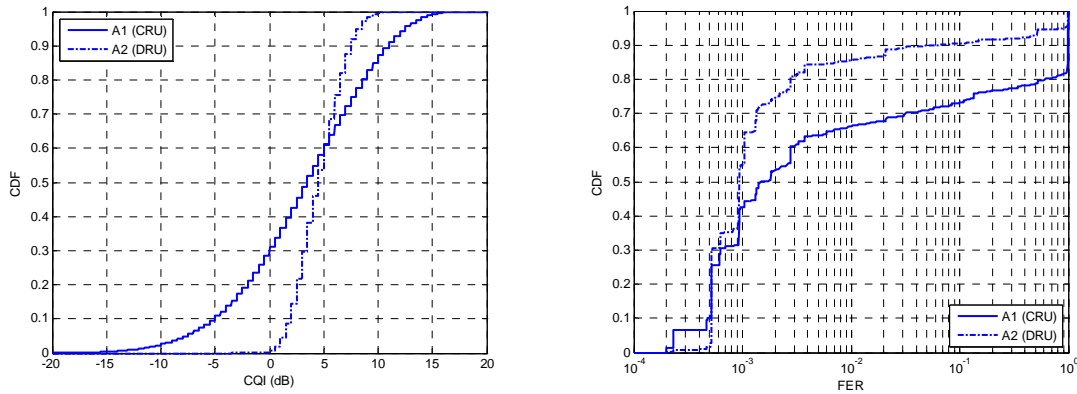


Figure 4-1: CDF of measured CQI (left) and FER (right) for scenarios A1 (CRU) and A2 (DRU).

Figure 4-1 shows the distributions of the CQI (left) and FER (right) measured by the users for CRU and DRU sub-channelization scenarios A1 and A2, respectively. As expected, the CQI distribution for DRU has much lower variance around a slightly higher mean. This is thanks to the diversity achieved by sub-carrier permutation for the DRU mode.

In term of FER, we can observe for DRU mode a much higher percentage (20% more) of users measuring an FER lower than scheduling threshold of  $10^{-2}$ . This reflects much better tracking capability in the DRU mode, which is expected since the CQI variation is much lower with DRU than with CRU (cf. CQI distribution), and thus the scheduler decision for the allocated resource units and MCS schemes remain valid across two time intervals. This observation suggests the need to implement a mechanism for CQI prediction, in order to render the scheduler decision more viable in all scenarios considered.

Figure 4-2 shows the distributions of average user throughput (left) and sector throughput (right) for scenarios A1 and A2. Both scheduled (as allocated by the scheduler) and measured (as perceived by the user) values are depicted, in order to stress out the tracking capability of the scheduler.

For the average user throughput (left), we can observe higher throughputs for DRU as compared to CRU. However, there is clearly higher percentage (25% more) of users with throughput null in the DRU mode. This means that some active users are not scheduled during the transmission time period. The starvation by the scheduler of cell edge users in the DRU mode benefits to the other users and thus increases the per-user average throughput. This starvation happens in the DRU mode because the users at the cell edge (with low SINR value) do not benefit from frequency selectivity across the whole bandwidth since DRU attempts to equalize the quality across the resource units.

The gap between CRU and DRU average user throughput becomes much greater when considering the throughputs measured by the users as compared to the scheduled throughputs. This is direct consequence of the better tracking capability in the DRU mode as compared to the CRU mode (see Figure 4-1 right). The CQI variation is much lower and thus the scheduler decisions are more viable, which results in much higher percentage of FER below the threshold of  $10^{-2}$ .

In term of sector throughput, the conclusions remain the same, and the gap is much higher, as we add-up the individual gaps for 10 users. Without CQI prediction, it is clear that DRU mode results in nearly 20% higher measured (or actual) sector throughput than in CRU mode.

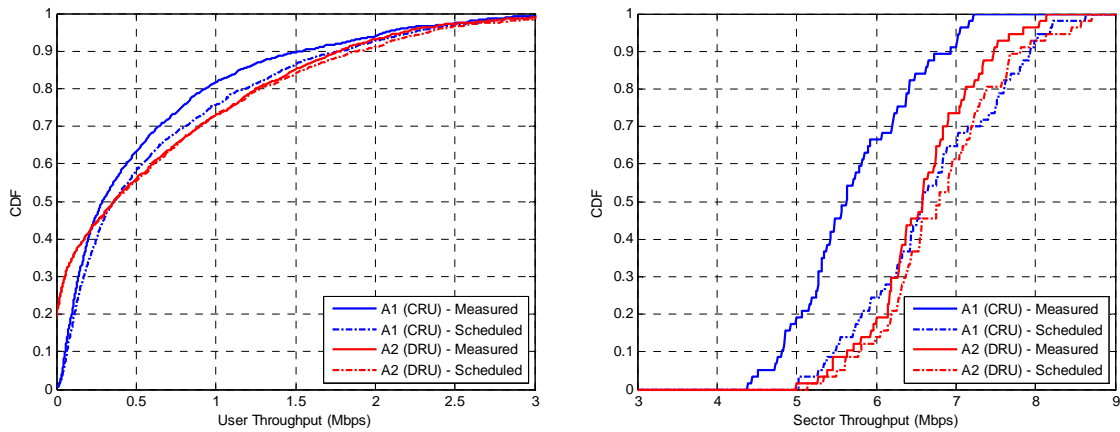


Figure 4-2: CDF of measured and scheduled user throughput (left) and sector throughput (right) for scenarios A1 (CRU) and A2 (DRU).

Figure 4-3 shows the distributions of the number of scheduler users per sector (left) and the number of resource units scheduled by user (right). As previously interpreted, we can observe nearly 20% less users scheduled in the DRU mode than in the CRU mode, which led to higher throughput per scheduler user, to the detriment of lower cell edge user throughput. This also transfers to the number of resource units scheduled by user, where higher number of resource units is assigned in DRU mode, but also higher number of users starting with no resource units allocated.

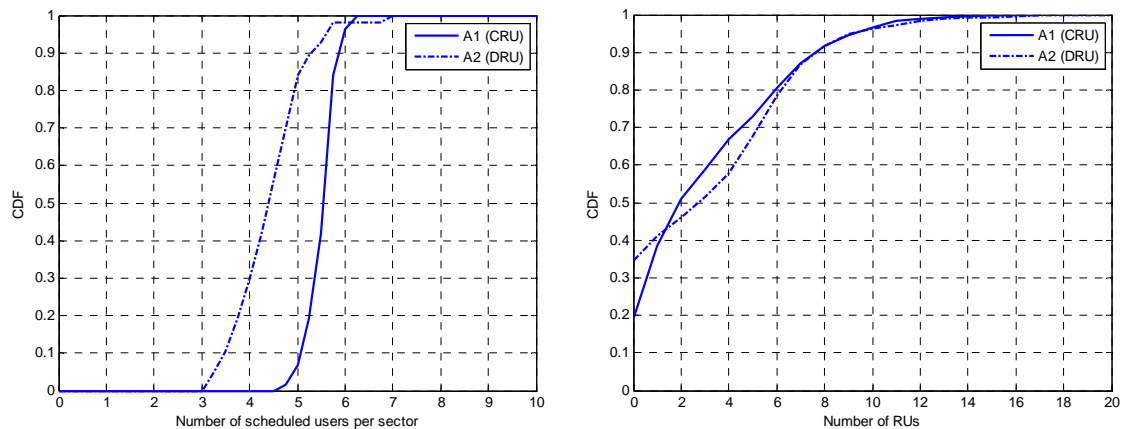


Figure 4-3: CDF of number of scheduled users per sector (left) and number of scheduled RU per user (right) for scenarios A1 (CRU) and A2 (DRU).

Figure 4-4 shows the average user throughput per distance, where the higher throughput in DRU mode previously observed transfers here. But this transfer does not happen evenly across the distance, where we can see lower gap (nearly 10%) in the area up to half of the cell radius from the base station, as compared to much higher gap (up to 50%) for further areas.

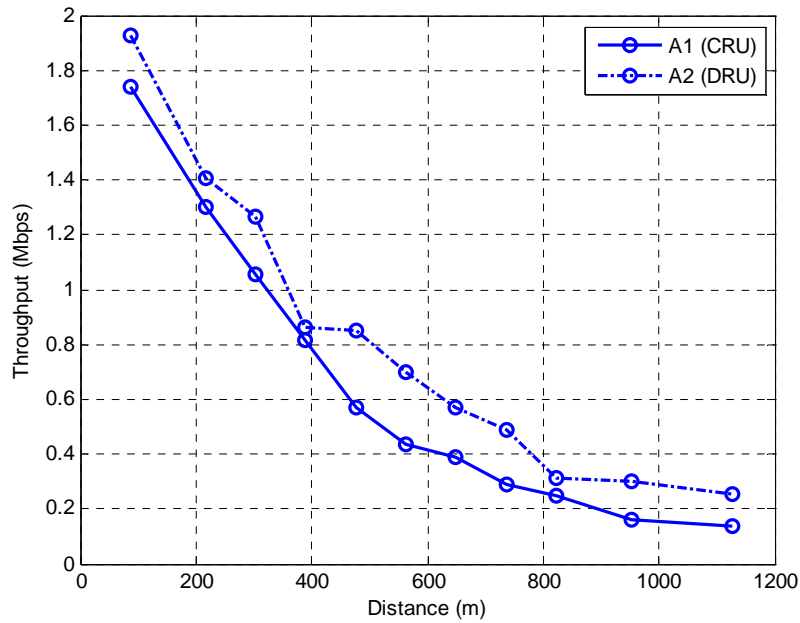


Figure 4-4: Average user throughput per distance for scenarios A1 (CRU) and A2 (DRU).

Figure 4-5 shows the average percentage of the MCS scheduled for users per distance. In both scenarios, we can clearly appreciate of more robust MCS schemes as the users get farther from the base station. On another hand, we can observe clearly much higher percentage of selection of coding rate 1/2 for all QPSK, 16QAM and 64QAM constellations. Furthermore, some MCS modes seem not to be selected at all, e.g. 16QAM 2/3, 3/4 and 5/6. This suggests to smartly reduce the number of modes for selection by the scheduler instead of just going for all possible combinations of coding rates and constellation orders.

Now comparing the CRU and DRU modes, we can clearly see the CRU mode to schedule more high throughput MCS (such as 64QAM 3/4 and 5/6) than DRU mode. This can be understood thanks to the higher range of CQI values reachable by the CRU mode, which benefits from frequency selectivity across the bandwidth, as compared to DRU mode which tries to equalize the CQI over the whole bandwidth.

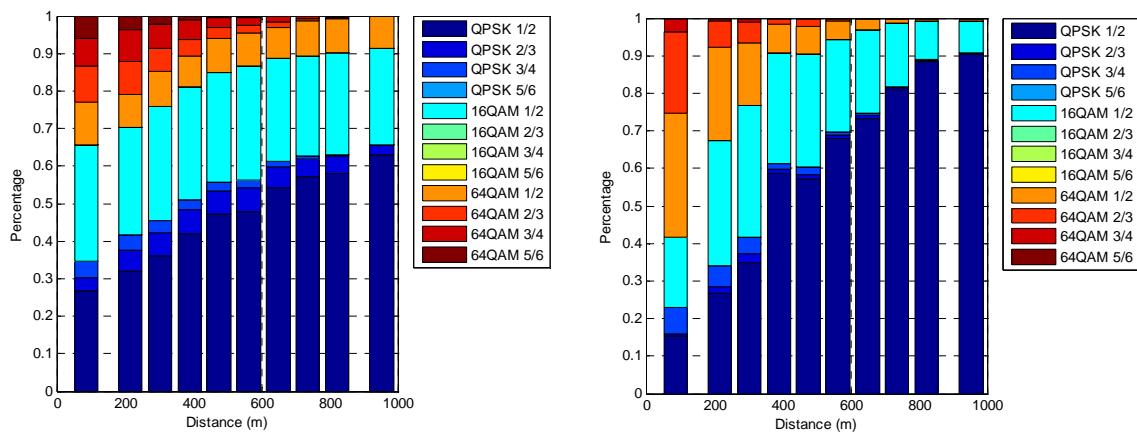


Figure 4-5: Percentage of MCS usage per distance for scenarios A1 (CRU) (left) and A2 (DRU) (right).

### 4.2.2 SISO vs. SIMO reception

Figure 4-6 to Figure 4-10 show statistics for different performance metrics comparing the scenario A with SISO (1 x 1) to scenario B with SIMO (1 x 2). Both CRU and DRU modes are also depicted.

Figure 4-6 shows the distributions of CQI (left) and FER (right) as measured by the users. For the CQI distribution, in both modes, we can appreciate the gain achieved by using SIMO as compared to SISO. In the CRU mode, this gain decreases as we move to the range of high CQI values, whereas in the DRU mode, the opposite occurs, i.e. the gain increases as when the CQI value increases. The effect of CRU and

DRU modes on SISO and SIMO stays the same as expected, meaning in that higher variance of CQI values for CRU modes thanks to its frequency selectivity across the resource units.

In term of FER, we can see that the lower the variance of the CQI values is, the better the FER distribution is, reflecting better tracking capability thanks to less channel quality variation over time. In the SIMO mode with DRU, the variance of CQI is higher than with SISO, which results in lower measured FER distribution reflecting lower capability of channel tracking.

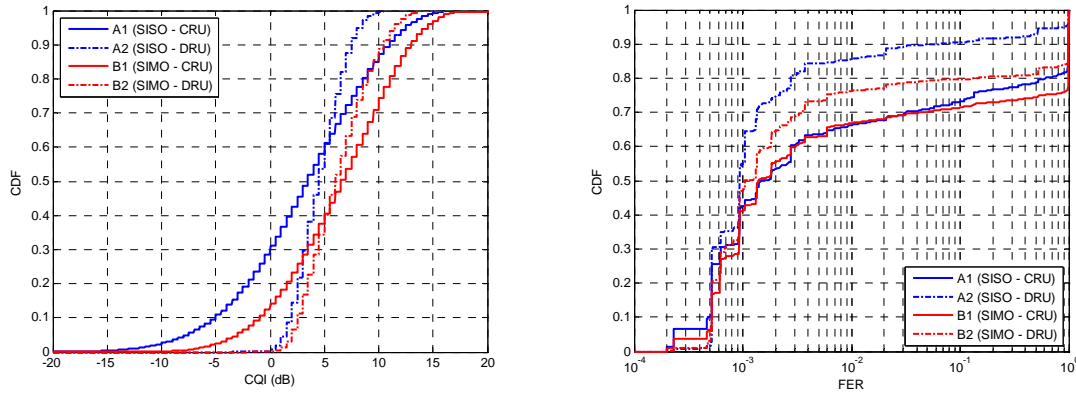


Figure 4-6: CDF of measured CQI (left) and FER (right) for scenarios A (SISO) and B (SIMO).

Figure 4-7 illustrates the CDFs of average user throughput and sector throughput for scenarios A (SISO) and B (SIMO). Only the throughput as measured by the users is depicted. In the CRU mode, we can clearly observe the gain achieved by SIMO as compared to SISO throughout the whole range of throughput values (we thus improve peak, average, and cell edge user throughputs). This gain is found to be nearly 20% in average.

In the DRU mode, we can see clear gain up to 70% of the CDF for throughputs up to 0.9 Mbps. The percentile of null throughputs reduces from nearly 20% to nearly 5% showing clear improvement on the cell edge throughput. For very high values of user throughput, the measured user throughput is found slightly better for SISO-DRU than SIMO-DRU due to the better channel tracking capability and thus lower FER values for SISO-DRU mode, which benefits from a lower CQI variation. Overall, in term of sector throughput, there is clear advantage of SIMO-DRU as compared to SISO-DRU, estimated to up to 12% in average. It is lower than the 20% achieved in the CRU mode due to the lower channel tracking capability for SIMO-DRU than SISO-DRU (cf. FER distribution in Figure 4-6 right).

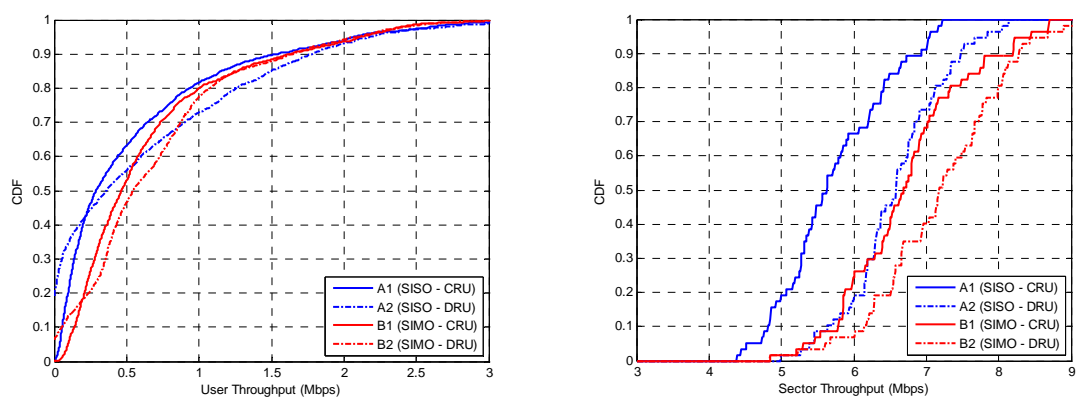


Figure 4-7: CDF of measured user throughput (left) and sector throughput (right) for scenarios A (SISO) and B (SIMO).

Figure 4-8 depicts the CDFs of the number of scheduled users per sector (left) and the number of resource units per user. We can clearly see higher number of scheduler users per sector in the SIMO mode, and the gap between CRU and DRU modes is reduced. This is direct result of the steady CQI improvement achieved by SIMO as compared to SISO. Thus more users share the resources at a time, which increases

the fairness of the scheduler. The more users sharing the resources at a time results in lower number of resource units assigned to each user, as it can be appreciated from the CDF of the number of resource units per user on the right. Much lower number of users are not allocated any resource unit (cf. percentage of number of resource units equal to 0) in the SIMO mode, whilst more users share the resource units at a time which results in lower maximum number of resource unit per user (from 12 to 8).

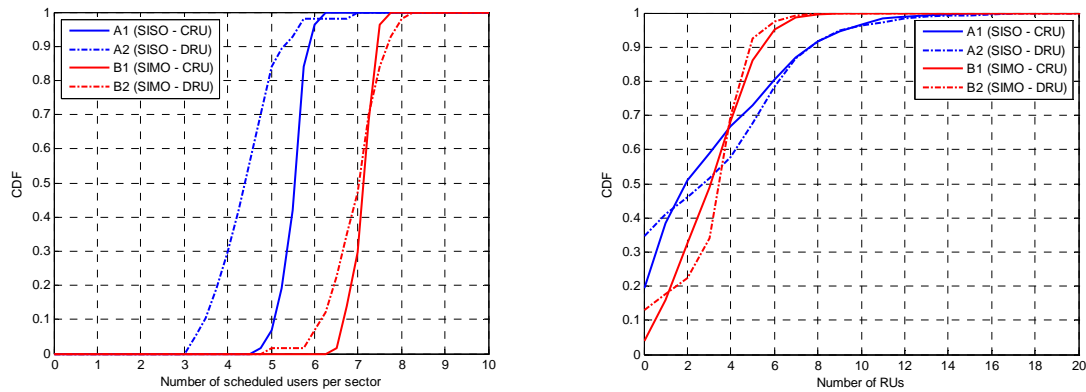


Figure 4-8: CDF of number of scheduled users per sector (left) and number of scheduled RU per MS (right) for scenarios A (SISO) and B (SIMO).

Figure 4-9 shows the average measured user throughput per distance for SISO and SIMO modes with CRU and DRU sub-channelization. Similar to Figure 4-4, we observe the gain achieved by the SIMO to increase as when the users get farther from the base station. This is expected as the users close by the base station already benefit from high CQI values without SIMO and thus selects the same high throughput MCS as in the SIMO mode. As the users move far away from the base station, the gain is then remarkably much higher, as the SIMO mode allows to select higher throughput MCS thanks to its higher CQI values. This is clearly highlighted in Figure 4-10 where the average percentage of MCS selection is illustrated per user distance from the base station.

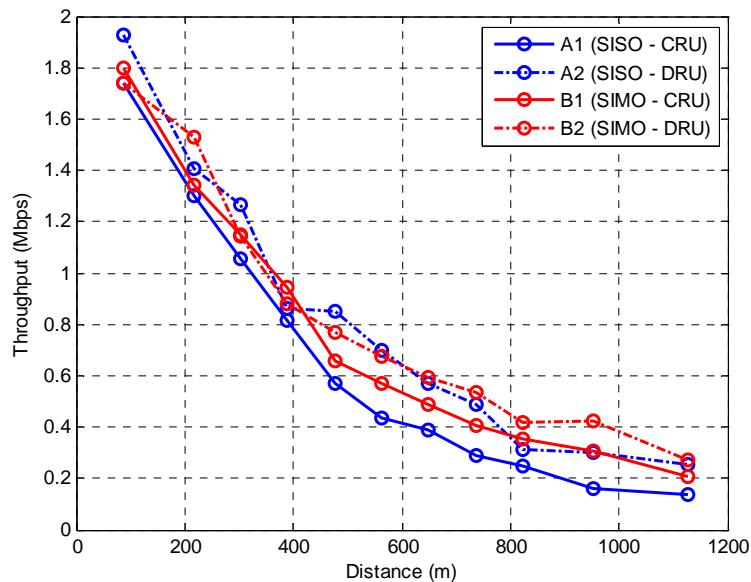


Figure 4-9: Average user throughput per distance for scenarios A (SISO) and B (SIMO).

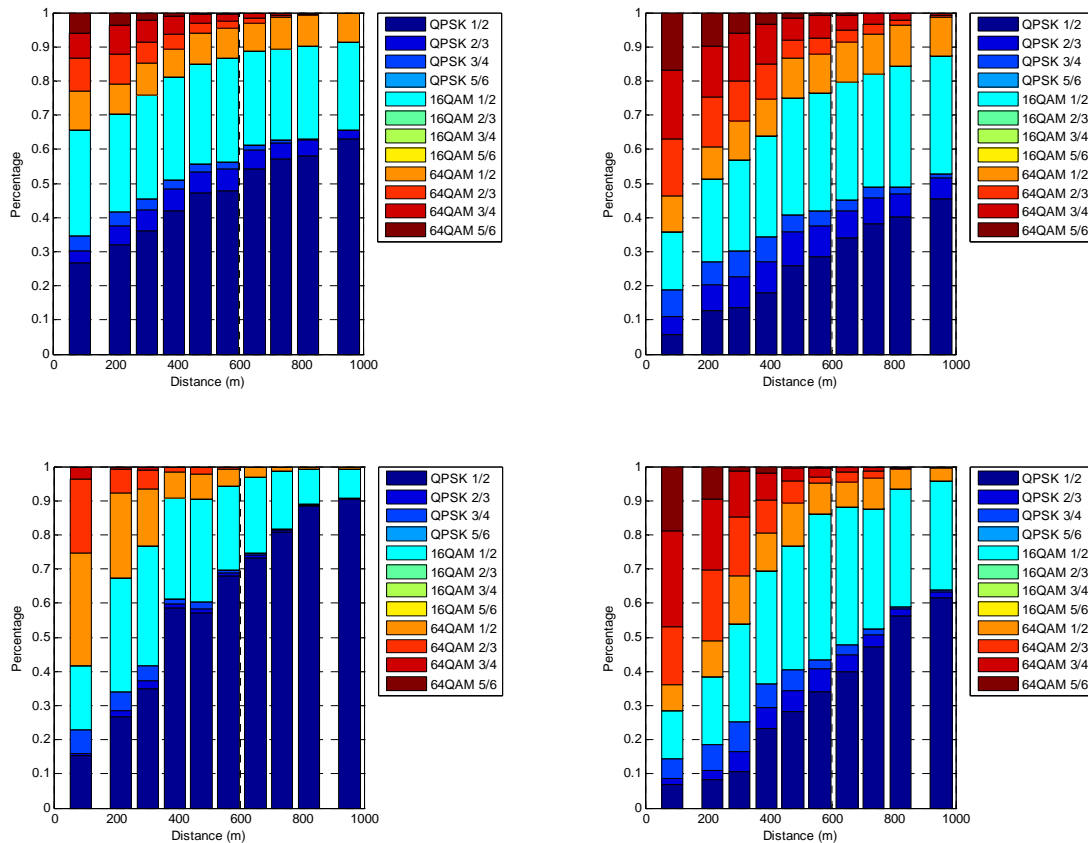


Figure 4-10: Percentage of MCS usage per distance for scenarios A1 (SISO - CRU) (top left), B1 (SIMO - CRU) (top right), A2 (SISO - DRU) (Bottom left), B2 (SIMO - DRU) (Bottom right).

### 4.2.3 Low mobility vs. Medium mobility

Figure 4-11 to Figure 4-15 show statistics for different performance metrics comparing the scenario A with Pedestrian B@3Kmh to scenario C with Vehicular A@30Kmh. Both CRU and DRU sub-channelization modes are considered.

The CDFs of measured CQI (left) and FER (right) are depicted in Figure 4-11. In the CRU mode, the CQI in PedB is found higher than in VehA. This is direct consequence of the time and frequency selectivity of VehA as it has lower channel coherence time (since higher speed) and also lower channel coherence bandwidth (since higher delay spread). This higher selectivity results into higher CQI variation.

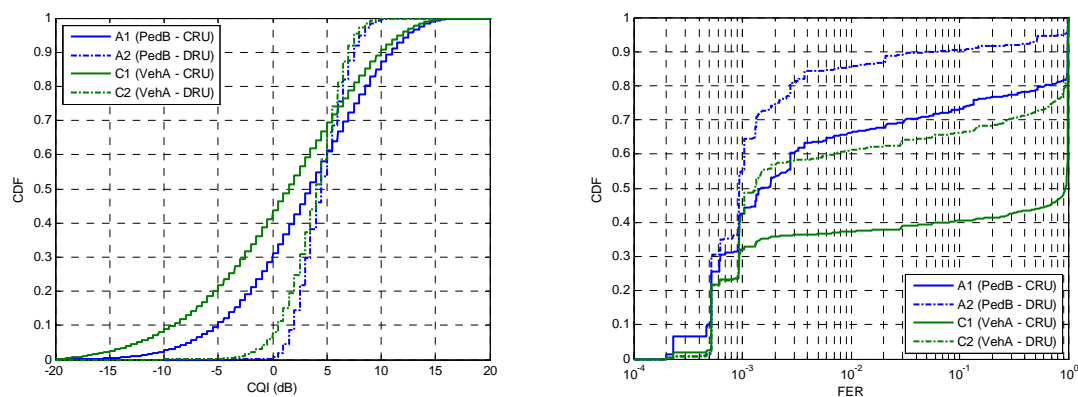


Figure 4-11: CDF of measured CQI (left) and FER (right) for scenarios A (PedB3) and C (VehA30).

The FER distributions on the right are the direct consequence of this higher CQI variation. In the CRU mode, where the maximum selectivity is obtained, the FER distribution is the lowest, reflecting the highest CQI variation confirmed by the CQI distribution on the left. This results in very low capability of

tracking the channel conditions, and thus clearly raises the need to implement the CQI prediction mechanism accounting for the time-correlation of the channel quality.

Figure 4-12 depicts the measured average user throughput and sector throughput for scenarios A and C. The lower CQI distribution of VehA scenario C results into clearly lower average user throughput and sector throughput for both CRU and DRU modes. The gap is much higher in the CRU mode as the DRU mode inherently reduces the time-frequency selectivity within the resource units by bringing the available diversity over the whole bandwidth into each of the resource units. Furthermore, the channel tracking capability in the CRU mode is much lower as shown in Figure 4-11, which makes the gap even higher. Overall, the performance loss for VehA scenario in sector throughput is nearly 50% in average for CRU mode, and nearly 25% for the DRU mode.

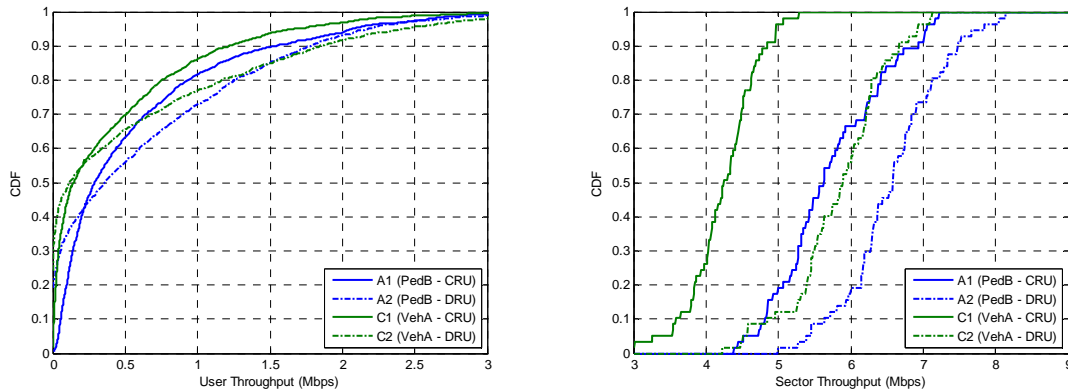


Figure 4-12: CDF of measured and scheduled user throughput (left) and sector throughput (right) for scenarios A (PedB3) and C (VehA30).

Figure 4-13 shows the CDFs of the number of scheduled users per sector (left) and number of scheduled resource units per user. It is clear the lower CQI values obtained in the VehA mode result into lower number of scheduled users at a time per sector and thus higher number of resource units scheduled per user. The number of users suffering starvation is obviously higher in VehA than in PedB.

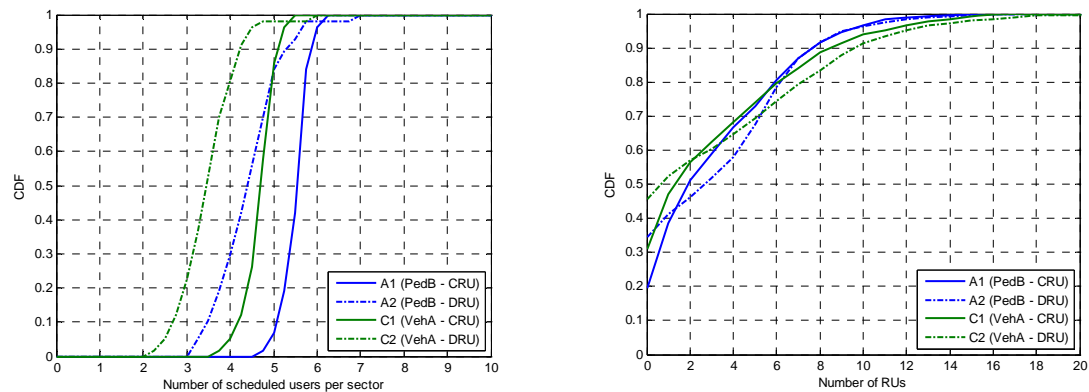


Figure 4-13: CDF of number of scheduled users per sector (left) and number of scheduled RU per MS (right) for scenarios A (PedB3) and C (VehA30).

Figure 4-14 and Figure 4-15 show the average user throughput and average percentage of MCS selection per user distance from the base station. In the CRU mode, we can clearly the scheduler in the VehA case to resort to robust MCS rather than high throughput MCS due to lower CQI values. This is less significant in the DRU mode, which achieves inherent diversity and results in relatively higher CQI values. As previously observed, the gap between different scenarios does not keep constant over the distance as the distribution of MCS selection also moves with distance. The closer the users are to the base station the

lower the gap is thanks to the use of close high throughput MCS modes, whereas the farther the users are from the base station the higher is the gap as the higher is the range of choice between the MCS.

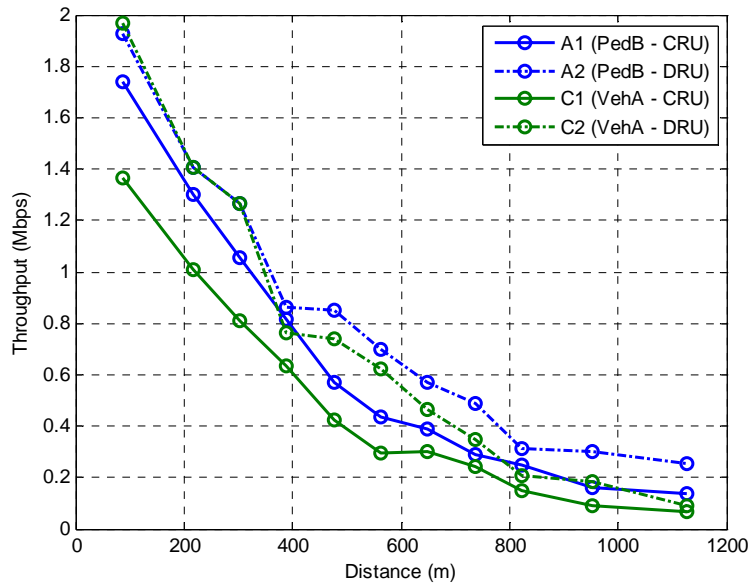


Figure 4-14: Average user throughput per distance for scenarios A (PedB3) and C (VehA30).

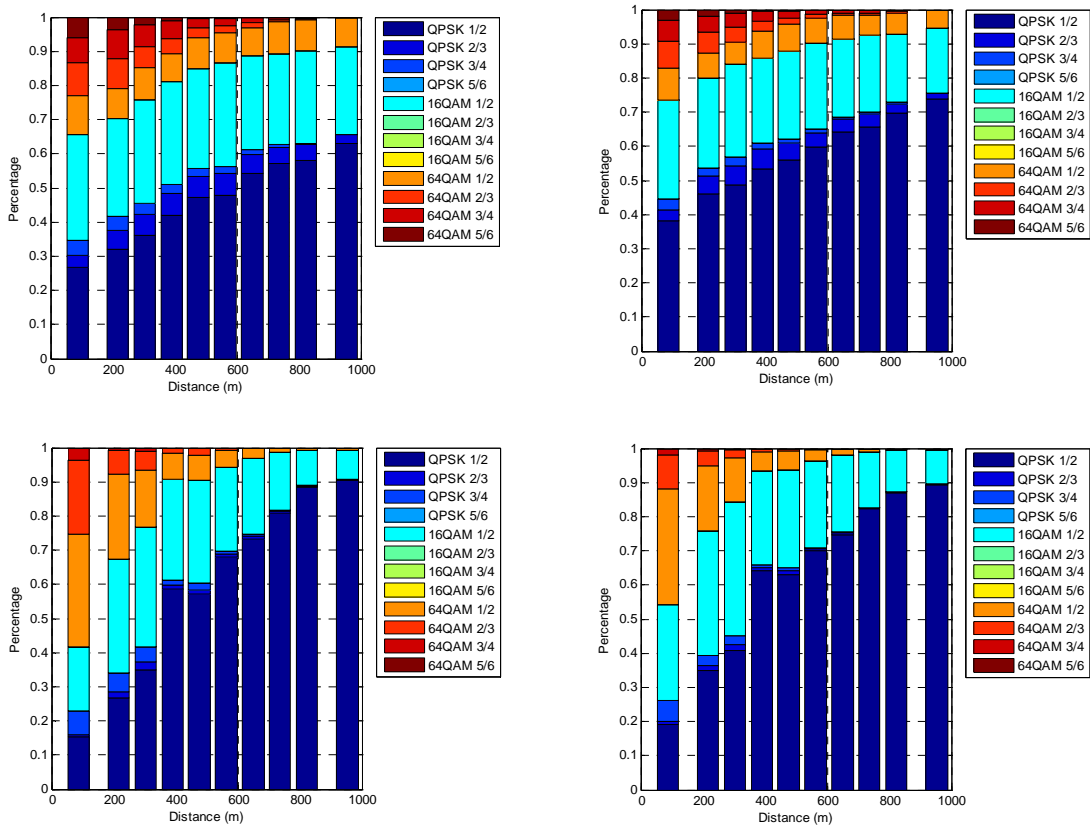


Figure 4-15: Percentage of MCS usage per distance for scenarios A1 (PedB3 - CRU) (top left), C1 (VehA30 - CRU) (top right), A2 (PedB3 - DRU) (Bottom left), C2 (VehA30 - DRU) (Bottom right).

## 5. Conclusions and Perspectives

In this report, we presented the first system level results using WiMAX IEEE 802.16m compliant system level simulator developed for the purpose of evaluating DAVINCI technologies at the system level. We highlighted the mutual information based link to system interface used to abstract the performance of link level technologies at the system level. A comparison was conducted between WiMAX IEEE 802.16m CTC and DAVINCI codes at the link to system interface. This led to the conclusions that DAVINCI codes achieve a slight gain (0.5 dB in the best case), which using the current link to system interface would yield to minor gain for DAVINCI at the system level. The DAVINCI codes are expected to achieve higher performance for higher codeword sizes, which if confirmed, might improve a little the gain observed at the system level. This is in the context of linear receivers. The gain might improve in the context of non-linear receivers, where DAVINCI is expected to be more suitable than other coding schemes. This is yet to be confirmed and then evaluated using adequate link to system interface that captures the benefits of DAVINCI codes in the context of non-linear receivers.

The results at the system level are obtained with WiMAX IEEE 802.16m CTC scheme. No results could be obtained with DAVINCI codes as the available parity check matrices do not cover the range of configurations needed for system level performance evaluation. We conducted the performance evaluation for contiguous vs. distributed sub-channelization, SISO vs. SIMO modes, and low vs. medium mobility scenarios. The results shown are coherent and give clear advantage for the distributed sub-channelization as compared to contiguous sub-channelization for two reasons. The first is due to the starvation of some users by the scheduler in the context of distributed sub-channelization, where the situation of bad user over all the resource units has higher occurrence than in the contiguous sub-channelization. This results in a lower cell edge throughput but higher throughput for the fewer scheduled users, since each them is assigned higher number of resource units than in contiguous case. The second reason is the lower CQI variation in the distributed case, since the sub-carrier permutation employed nearly equalizes the CQI values across the resource units. This results in a higher capability of the scheduler to track the channel, and thus the scheduler decisions remain viable from one TTI to another. This second reason is emphasized by comparing the performance with Pedestrian B@3Kmh to Vehicular A@30Kmh, where the higher CQI variation due to higher time-frequency selectivity drastically reduces the capability of the scheduler to track the channel. This raised the need to implement CQI prediction mechanism that accounts for the time correlation between adjacent TTIs. This is left for future work.

On another hand, comparing SISO and SIMO (1x2) modes showed significant gain for the SIMO of up to 20%. Performance evaluation and comparison with other MIMO modes (e.g. space-time coding, spatial multiplexing) are left for future work.

Finally, it is worth pointing out that the system level simulator does not implement H-ARQ. We clearly showed that even in the scenarios of good channel tracking capability, there is 10 to 15% measured FER higher than FER threshold of  $10^{-2}$ . By implementing the H-ARQ, this percentage will be reduced, and the reduction will transfer to other relevant system level performance metrics such as the number of re-transmissions and latency. This is also left for future work.

## References

- [TGm-EMD] IEEE 802.16m, "Evaluation Methodology Document (EMD)," IEEE 802.16m-08/004r5, 15 January 2009.
- [TGm-SDD] IEEE 802.16m, "System Description Document (SDD)," IEEE 802.16m-08/003r8, 10 April 2009.
- [DAV-D221] DAVINCI, "Link Level Evaluation, Issue 1", FP7-DAVINCI deliverable D2.2.1, 30 November 2008.